

Received January 17, 2022, accepted February 4, 2022, date of publication February 7, 2022, date of current version February 22, 2022.

Digital Object Identifier 10.1109/ACCESS.2022.3149893

Development and Implementation of Energy-Efficient Magnetorheological Fluid Bypass Damper for Prosthetics Limbs Using a Fuzzy-Logic Controller

N. H. DIYANA NORDIN¹, ASAN G. A. MUTHALIF^{1,2}, (Senior Member, IEEE),
M. KHUSYAIE M. RAZALI¹, ABDELRAHMAN ALI^{1,2}, AND AYMAN MUSTAFA SALEM^{1,2,3}

¹Smart Structures, System and Control Research Laboratory (S³ CRL), Kulliyah of Engineering, International Islamic University Malaysia, Kuala Lumpur 53100, Malaysia

²Department of Mechanical and Industrial Engineering, Qatar University, Doha, Qatar

³Department of Mechanical Engineering, Faculty of Engineering, University of Malaya, Kuala Lumpur 50603, Malaysia

Corresponding author: Asan G. A. Muthalif (drasan@qu.edu.qa)

This work was supported in part by the International Research Collaboration under Grant IRCC-2020-017 and Qatar University Graduate Assistantships Grant. The Open Access funding has been provided by the Qatar National Library, Qatar.


ABSTRACT Walking behaviour in amputees with lower-limb loss is absent from shock-absorbing properties. A damper can be used to reduce the impact of ground reaction force (GRF) during heel strikes. Magnetorheological fluid (MRF) damper is deemed the best option for this application as it includes the advantages of both passive and active dampers. An enhanced MRF damper is essential in supplying the appropriate current and damping force levels. Therefore, an energy-efficient design is required to prolong the battery life used by MRF dampers in prosthetic limbs. This paper investigates two fluids of different properties and magnetic particle volume content. A bypass damper was used to observe the response of both fluids. The findings highlighted that an MRF with a higher percentage of solid weight could produce a more significant damping force with a lesser amount of applied current. This work presents a simulation study on implementing the energy-efficient MRF damper utilizing a Fuzzy-PID controller in a prosthetic limb.

INDEX TERMS Energy efficiency, magnetorheological fluid, magnetic particle ratio, prosthetic limb, shock absorption.

I. INTRODUCTION

The knee behaves as the primary shock absorber in a healthy human lower limb. The tendons also serve as a shock absorber during initial contact, protecting muscles against damage from rapid and forceful lengthening during energy dissipation [1]. Interestingly, women absorb more energy during landing due to their landing posture [2]. Thus, losing a lower limb affects an amputee's mobility, health and quality of life.

The use of powered devices to mimic the function of a leg exhibit superior performance as they are controlled with microprocessor, sensors and mechanical devices [3]–[5]. As a result, such devices are usually large, expensive, and require significant power sources [6]–[8]. Dynamic and static stability are crucial design considerations [9], [10].

The associate editor coordinating the review of this manuscript and approving it for publication was Muhammad Zakarya .

While providing variable stiffness and damping is the priority, numerous studies are conducted to minimize total energy consumption via elastic actuation modification [11]–[13] and utilize both passive and active modes [14], [15].

Magnetorheological fluid (MRF) is a smart material capable of changing its damping characteristic. The rheological property of the fluid varies with the presence of a magnetic field, and it has made it beneficial in various applications. Figure 1 shows the arrangement of magnetic particles with and without a magnetic field. The magnetorheological response depends strongly on the physical (size, distribution, and shape) and magnetic (saturation magnetization) nature of the particles in MRF [16]. The application of MRF can be found in elevators [17], industrial shock absorbers [18], seismic response reduction devices [19], [20], vehicle suspension systems [21], [22], stab or bullet resistance vests [23], [24] and rehabilitation devices [25]–[27]. Recent advances in the

literature showed good applications in engine mounts, crash protection seats, brakes, and clutches [28].

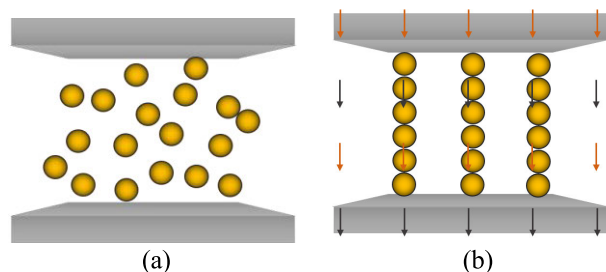


FIGURE 1. The arrangement of the magnetic particles, (a) without magnetic field: the magnetic particles are suspended randomly in the matrix material. (b) with magnetic field: the particles are uniformly distributed along the direction of the magnetic field.

The stiffness and damping properties of the human lower limb change throughout the gait cycle. By manipulating the properties of MRF for natural gait, employing an MRF damper in a prosthetic limb may assist amputees in their daily activities. Tuned magnetic fluid dampers are often used in the vibration reduction of structures due to their high stability and quick response to vibration. Numerous studies have successfully demonstrated the prospects of MRF damper in prosthetic limbs [29]–[34]. An MRF damper does not need a significant power source, as the power required is only used for magnetic field generation. However, power consumption optimization studies must be carried out to prolong battery use. This enhancement is crucial to designing an energy-efficient MRF damper, which aims at consuming less energy without reducing the performance of a device.

Previous studies were able to identify the challenges in MRF-based dampers. One of the challenges found in MRF dampers is the fluid particle separation which occurs when the particles radially separate perpendicular to the direction of the compressive force in the squeeze mode. Ismail *et al.* [35] studied fluid behaviour when subjected to compressive forces. They concluded that fluid separates from the particle phase, changing the particle chain structure and causing pressure build-up due to increased resistance to compressive force. Temperature impacts on MRF have resulted in viscosity changes, as the latter is temperature-dependent. Depending on the application, the operating temperature for MRF may range from $-20\text{ }^{\circ}\text{C}$ to $150\text{ }^{\circ}\text{C}$. Chen *et al.* [36] studied the effects of temperature on MRF and proposed a relation between the two variables. Furthermore, sealing troubles in MRF are caused mainly by a decrease in oil viscosity, which is typically caused by an increase in temperature. Cylindrical seals have been used to overcome fluid leakage due to sudden changes in viscosity [37]. Other challenges are associated with the preparation and use of MRFs, such as the formation of hard cake that results from the agglomeration of magnetic particles and remnant magnetization. This defect remains after the magnetic field is turned off, resulting in the non-homogeneous behaviour of MRF. Moreover, a clumping effect arises from a very high magnetic field applied for

a long time that causes the entrapment of particles in the form of chains letting the carrier fluid flow freely behind the magnetic particles. Additionally, magnetic particles are prone to oxidization, which causes rusting of the magnetic particles, affecting the performance of the MRF [38].

This work explores the implementation of MRF damper in transtibial (below the knee) prosthetic limb utilizing adaptive control techniques. A fuzzy-PID controller is implemented to obtain the system's response and ensure that the damper performs efficiently. Additionally, the work involves an experimental investigation to observe the effect of changing the particle ratio on the fluid's viscosity. Here, the change of the viscosity is observed through the change of the force, as measured by the sensor embedded in the universal testing machine (UTM).

The arrangement of the paper is as follows; Section 1 introduces the research conducted in this work, Section 2 presents kinematics derivations of the human lower limb based on the link-segment model, Section 3 discusses the experimental setup and results. Section 4 shows the implementation of the energy-efficient MRF damper in a prosthetic limb with a fuzzy-PID controller. Finally, Section 5 concludes the work done in this paper.

II. RELATED WORK

Issues in designing energy-efficient MRF dampers can be addressed via damper designs and fluid optimizations. Hu *et al.* [39] and Nie *et al.* [40] studied different piston configurations to maximize the dynamic range. Dominguez *et al.* [41] focused on the piston head while Krishna *et al.* [42] and Gurubasavaraju *et al.* [43] optimized the effect of the fluid flow gap. Desai and Upadhyay [44] optimized the magnetorheological properties of aqueous magnetic fluids by adding mono-dispersed silica nanoparticles. Parameters such as flange length, gap width, piston head housing thickness, the radius of piston core, and gap length are often optimized using software before being fabricated. Parlak *et al.* [45] used ANSYS, a finite element software, while Singh *et al.* [46] and Nanthakumar *et al.* [47] used an optimization algorithm to optimize the geometrical parameters of the damper. Basically, in terms of the design, modifications are done to increase the generated magnetic flux density with a given value of applied current.

Other studies have focused on exploring the parameters that affect the characteristics of the MRF. These studies have investigated the microscopic characteristics of MRF in magnetic fields [48], [49]. For example, Wang *et al.* [50] studied the microscopic characteristics of MRF suspensions. They deduced that the particle chain length of the MRF with a high particle volume fraction increases sharply with magnetic fields. Wu *et al.* [51] investigated the effect of particles based on their distribution. They conclude that larger particle size increases the impact of MRF due to the more robust assembling microstructure under the applying magnetic field. However, larger particles are prone to sedimentation due to gravitational force. In addition, faceted particles perform

better in particle shape, as the contact surface between the particles is larger. The sedimentations stability characteristics of MRFs can be efficiently improved by using lubricating additives or by adjusting the volume fraction of magnetic particles and the mass fraction of surfactants. Dispersibility of the iron particles can be enhanced by the addition of iron naphthalate and iron stearate. At the same time, sedimentation is typically controlled by using thixotropic agents and surfactants such as xanthan gum, silica gel, stearates, and carboxylic acids [52]. The use of MRF damper in prosthetic limbs, which provides a wide dynamic range, seems to prevent these conditions from happening due to its response to the magnetic field. The MRF capability of altering its rheological property and changing its viscosity when subjected to the intensity of the external magnetic field allows covering the advantages of both passive and active dampers due to this property.

III. MATHEMATICAL MODELLING OF HUMAN LOWER LIMB WITH MRF DAMPER

The linkage model of a healthy human lower limb is shown in Figure 2(a). Figure 2(b) shows the body centre of mass (COM) trajectory of the thigh, shank, and foot, grounded at the hip joint.

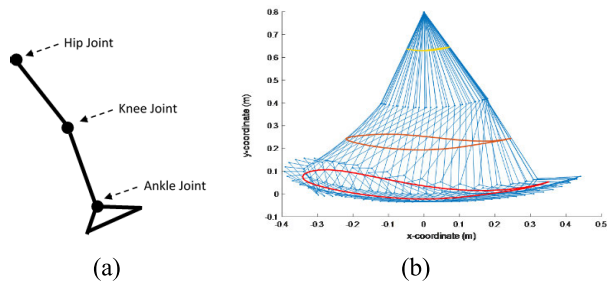


FIGURE 2. (a) Human lower limb link-segment model (b) Simulation of the human lower limb in one gait cycle, grounded at the hip joint.

In general, the equations of motion for i -th human lower limb segment can be expressed as:

$$m_i a_i = \sum_{i=1}^3 F_i = \sum_{i=1}^3 F_{ji} + F_{ei} + F_{gi} \quad (1)$$

$$I_i \ddot{\theta}_i = \sum_{i=1}^3 T_i = \sum_{i=1}^3 T_{ji} + T_{ei} + T_{gi} \quad (2)$$

where m_i is the mass of link i , a_i is the acceleration of link i , I_i is the mass moment of inertia of the body. The forces (f_i) and the net muscle moment acting on each joint (T_i), are subject to the external forces (F_{ei} , F_{gi}) and forces from muscle or tendon (F_{ji}).

The attachment of the MRF damper is shown in Figure 3(a). In the simulation studies, only the sagittal plane was considered. It is assumed that the joints of the rigid segments are frictionless. It is also assumed that the foot cannot rotate freely at the ankle joint without an MRF damper

and parallel spring. The MRF damper is powered on upon heel striking and remains at the “ON” state throughout the stance phase. The spring is at its original length when the user stands straight, i.e. the hip and knee angle is zero. The spring compresses before the foot is flat, and the compression length depends on the ankle flexion angle. During terminal stance and toe-off, the potential energy stored in the parallel spring will assist the user in pushing off.

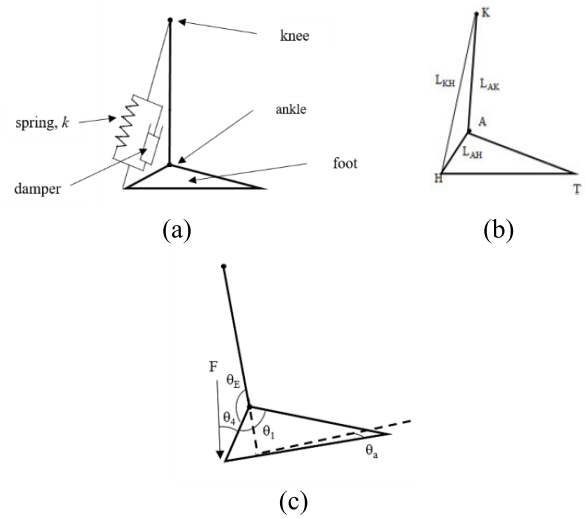


FIGURE 3. Simplified model of a transtibial prosthetic limb with linear MRF damper. (a) attachment of the MRF damper, (b) length of the segments; knee (K), ankle (A) and heel (H), (c) Ankle angle θ_a , hip joint angle θ_h and knee joint angle θ_k .

In Figure 3(b) and (c), L represents the length of the segment and denominator KH , AK and AH refer to the segments connecting knee (K), ankle(A) and heel (H), (c) Ankle angle θ_a , hip joint angles (θ_h and θ_k , respectively) is written as Eq. (3).

$$\theta_a = \frac{\pi}{2} - \theta_{3,ic} + \theta_2 - \theta_c \quad (3)$$

where $\theta_{3,ic}$ is the angle between the vertical line and the segment connecting ankle joint to toe, at standing still or double support and θ_c is the angle that the ankle-toe segment made with the horizontal line. At $\theta_a = 0^\circ$, $\theta_{3,ic} + \theta_c = 0$. Since, $\theta_2 = \theta_h + \theta_k$, thus, Eq. (3) becomes:

$$\theta_a = \frac{\pi}{2} - \theta_{3,ic} + \theta_h + \theta_k - \theta_c \quad (4)$$

The damper and parallel spring produce a linear force, F which translates into torque around the ankle joint, $\tau_{ankle\ output}$ that holds the foot to the desired ankle angle, using Eq. (5).

$$\tau_{ankle\ output} = FL_d \quad (5)$$

The moment arm, L_d is defined as:

$$L_d = L_{AH} \sin\theta_a \quad (6)$$

where,

$$\sin\theta_4 = \pi - \theta_E - \cos^{-1} \frac{L_{KH}^2 + L_{AK}^2 - L_{AH}^2}{2 \times L_{KH} \times L_{AK}} \quad (7)$$

IV. EXPERIMENTAL SETUP

The essential criteria of an energy-efficient MRF damper require a certain level of damping force produced by a minimum allowable applied current. Two fluids of different properties were investigated to determine which fluid performs better. A customized damper was used to facilitate the process of changing the fluid. The damper was then filled with one fluid type and tested at different applied current and stroking velocity levels. Using the obtained experimental results, the fluid that is best used to achieve an energy-efficient MRF damper in the application of prosthetic limb is chosen. The results obtained are presented in the subsections below.

A maximum of 1.5A of applied current, with an increment of 0.1A, was supplied to the electromagnetic coil to vary the magnetic field generated. The readings taken at the pole (bottom) of the electromagnetic coils are three to four times higher than the piston's side.

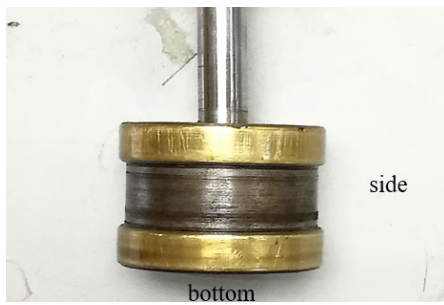


FIGURE 4. Measurements were taken at two faces, side and bottom of the piston head.

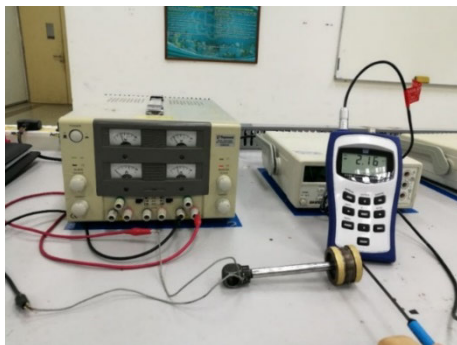


FIGURE 5. Measuring the amount of magnetic flux density generated by using a gaussmeter.

A. MAGNETIC FIELD PROFILE OF THE PISTON HEAD

The experiment was initiated by measuring the magnetic flux density generated by the coil. The piston's housing material was chosen to permit magnetic flux density through

the material. Readings were taken at both sides and bottom surfaces of the piston head (Figure 4) and listed in Table 1. FW Bell 5180 gaussmeter (Figure 5) was used to capture the strength of the magnetic flux density, passing through the steel housing of the piston. Particles suspended in the fluid will respond to the intensity of the flux.

TABLE 1. Magnetic flux density generated by the piston head of the MRF damper used.

Applied Current (A)	Magnetic flux density (mT)	
	Side	Bottom
0.1	0.07	0.21
0.2	0.15	0.46
0.3	0.22	0.79
0.4	0.35	1.13
0.5	0.39	1.48
0.6	0.41	1.69
0.7	0.46	2.10
0.8	0.52	2.30
0.9	0.63	2.64
1.0	0.85	2.93
1.1	1.11	3.15
1.2	1.20	3.63
1.3	1.57	3.87
1.4	1.62	4.29
1.5	1.71	4.92

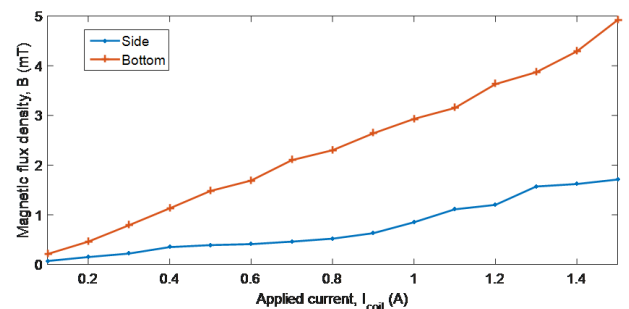


FIGURE 6. Graphical representation of the current varying magnetic field.

B. FORCE RESPONSE OF MRF DAMPER

An experiment was conducted with two different types of magnetorheological fluid (MRF-122EG and 132DG) from LORD Corp, with properties given in Table 2. Here, the term 'solid content by weight' was used. It represents the percentage of the ratio of solid particles suspended in the fluid to the total mass of the solution. A drop of each fluid was placed under the National DC5-163 compound biological microscope to observe the distribution of the magnetic particles in the fluid. In general, it is seen that the content of MRF-132 DG is denser compared with MRF 122-EG, as in Figure 7. As MRF-132 DG is thick, only a thin layer was put on the glass slide to permit light transmission through the specimen. The difference in solids content by a weight

inside the fluid results in the different viscosity values of the two fluids.

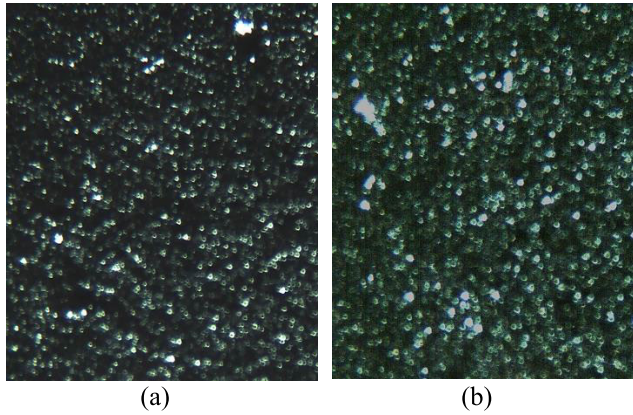


FIGURE 7. (a) MRF-122 EG and (b) MRF-132DG under the microscope.

TABLE 2. Properties of the MRFs used.

Properties	Types of MRF	
	MRF-122EG	MRF-132DG
Viscosity, Pa-s	0.042	0.112
Density (g/cm ³)	2.28	2.95-3.15
Solids content by weight - volume, (%)	72 – 31.6	80.98 – 27.5
Operating temperature, °C	-40 to +130	

A power supply was used to apply 0.1A to 1.5A current to the MR damper, incrementing 0.1A. Instron 3367 tensile test machine captured the force response in compression mode, as shown in Figure 8. The piston was moved downwards 30 mm at three-speed levels: 300 mm/min, 400 mm/min, and 500 mm/min.

Figure 9 displays the damping force of MRF-132DG, subjected to three different piston velocities, with applied 1.2A. Other data also depicts the same trend, and thus, an explanation using this graph is sufficient to represent the whole data. In general, four phases (Phase 1- Phase IV) can be seen on every plot.

During Phase 1, the rising of the force is to overcome the effect of inertia. A phase II, a similar trend is also observed. Here, the movement of the piston is restricted as the initial position of the piston head blocks the first opening of the bypass duct (Figure 10 (a)). Thus, a more significant force is required to move the fluid due to pressure differences in the bypass duct. When the piston travels around 0.7 mm (Figure 10 (b)), the piston unblocks the opening, resulting in a smoother fluid flow entering the bypass duct. Hence, the load gradually reduces, which subsequently reaches a steady state. However, in Phase IV, a slight force increment is observed at the end of the stroke length. More particles are present per

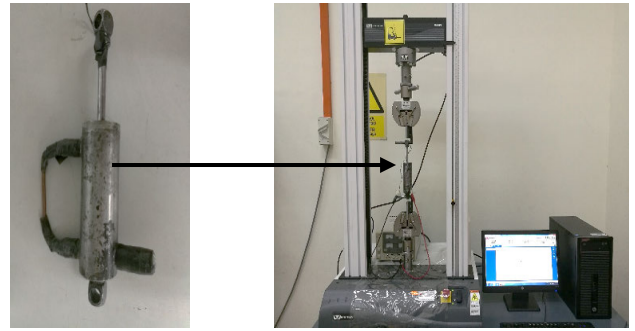


FIGURE 8. Experimental setup showing the tensile testing machine (Instron 3367) and the MRF damper.

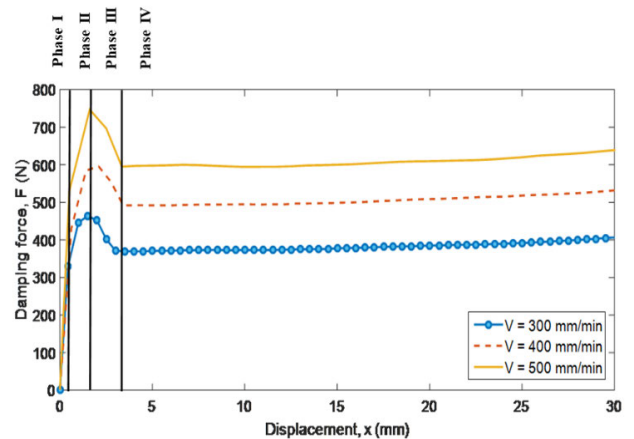


FIGURE 9. Damping force generated by MRF-132DG at 1.2A of applied current at three different velocities.

unit volume of fluid in this region as more fluid is pushed into the bypass duct, leaving some particles behind.

Figure 11 and Figure 12 show the force response of the MRF damper at three different velocities, travelling 30 mm downwards. The force plotted is in the operating region, i.e., in between the two openings of the duct. The viscosity of MRF-122EG is lesser than MRF-132 DG, and thus, a lower force is expected. Also, the higher the velocity of the piston, the higher the resulting damping force. As the current increases, the magnetic field generated increases. Thus, the field’s existence enhances the interaction between the particles, which increases the fluid’s resistance to flow. This effect can be seen through the tensile and compression force values that grow with the increment of the applied current.

Figure 13 displays the damping force generated at the end of stroke position ($x = 30\text{mm}$) for every current and stoking velocity. In the simulation study given in section 4, the weight of the leg is taken as 14.47kg. Using equations in Section 2, 106.24 N of damping force is needed at heel strike. Figure 13 was zoomed and shown in Figure 14, focusing on the region where the damping force is between 100N and 110N, suitable MRF is identified.

From Figure 14, the value of the damping force required (106.2N) can be generated at several velocities and currents,

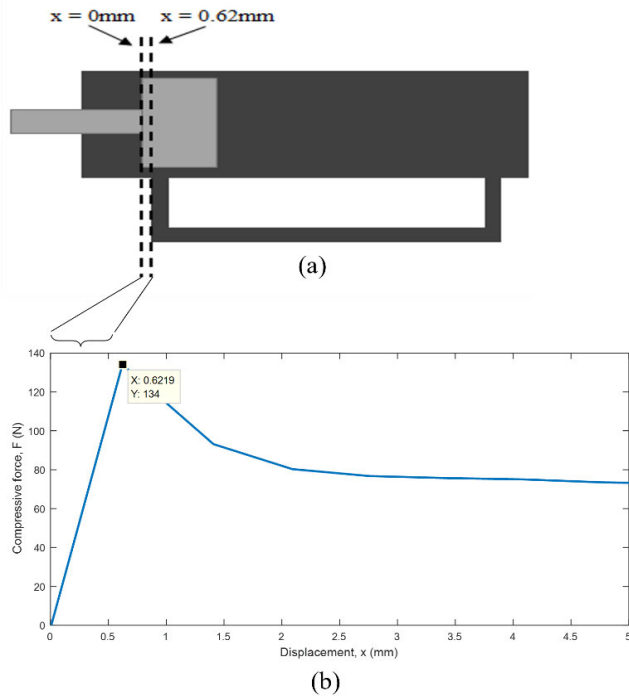


FIGURE 10. (a) The initial position of the piston. (b) The location of the piston when the force is at its highest.

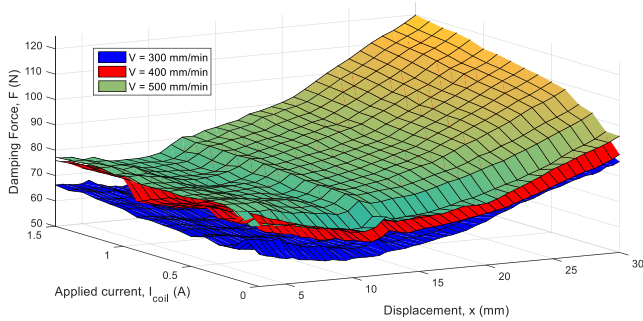


FIGURE 11. The compression force of the MRF damper, filled with MRF-122 EG at three different velocities.

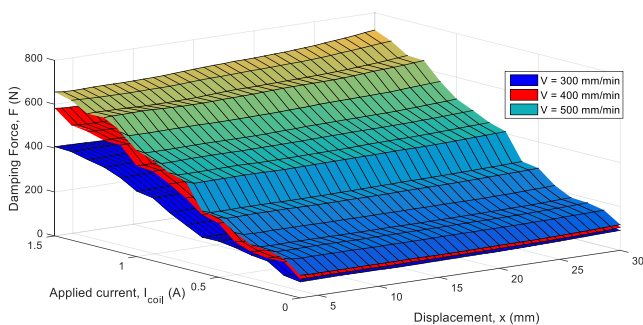


FIGURE 12. The compression force of the MRF damper, filled with MRF-132 DG at three different velocities.

as listed in Table 3. In general, MRF-132DG needs a lower amount of current to produce the same damping force, e.g., at 300mm/min, MRF-122EG needs as high as 1.485A to

TABLE 3. Various amounts of current to produce 106.2N.

MRF	Applied current, I_{coil} (A)	Stroking velocity, V (mm/min)
MRF-132DG	0.002	400
	0.099	300
	0.357	500
MRF-122EG	1.036	400
	1.485	300

TABLE 4. Fuzzy PID controller decision rules.

$de(t)$	$e(t)$				
	NB	NM	Z	PM	PB
	NB	NB	NB	NM	PM
NM	NB	NM	Z	PM	PB
Z	NM	NM	Z	PM	PB
PM	NM	NM	Z	PB	PM
PB	NM	NM	PM	PB	PM

TABLE 5. Intervals are assigned to the input and output of the F-PID controller.

Input variable	Interval
Error, $e(t)$	[-0.005,0.005]
Rate of change of error, $de(t)$	[-1.5,1.5]
Output variable	Interval
K_p	[0,50]
K_i	[0,35]
K_d	[0,40]

generate 106.2N, compared to 0.099 A for MRF-132DG. Hence, MRF-132DG is a better fluid to achieve an energy-efficient MRF damper for this case.

V. IMPLEMENTATION USING A FUZZY-PID CONTROLLER

In this section, a fuzzy PID controller is developed for the energy-efficient MRF damper. The control system block diagram of the MRF damper in the transtibial prosthetic limb is shown in Figure 15. A look-up table comprised of the actual data obtained during the experiment represented the MRF damper. The use of the look-up table reduces the complexity of deriving mathematical equations to model the damper.

The block diagram arrangement in MATLAB Simulink is displayed in Figure 16. It is assumed that before the foot is flat, the application of GRF is concentrated at the heel. On the other hand, the GRF is applied at the toe after foot flat. Upon heel striking, the leg, which acts as a shock absorber, automatically bends to reduce the impact of GRF. As the amount of ankle flexion angle depends on the knee and hip flexion angle thus, the spring compresses to the value that corresponds to the ankle angle, which is dependent on the thickness of the fluid. As the ankle flexion angle reaches zero, the piston gradually decreases its stroke and moves towards its initial position.

The controller’s performance is crucial at this stage as the collision between the foot and the ground happens in

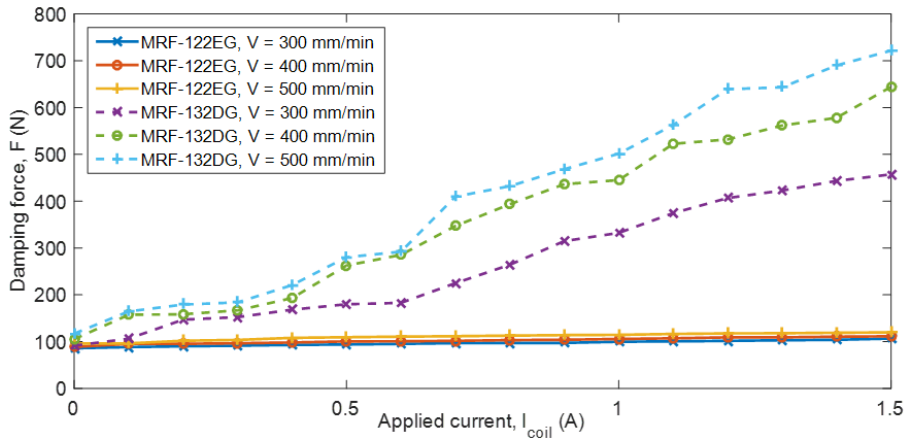


FIGURE 13. Damping force generated by the MRF damper at 30 mm of stroke length.

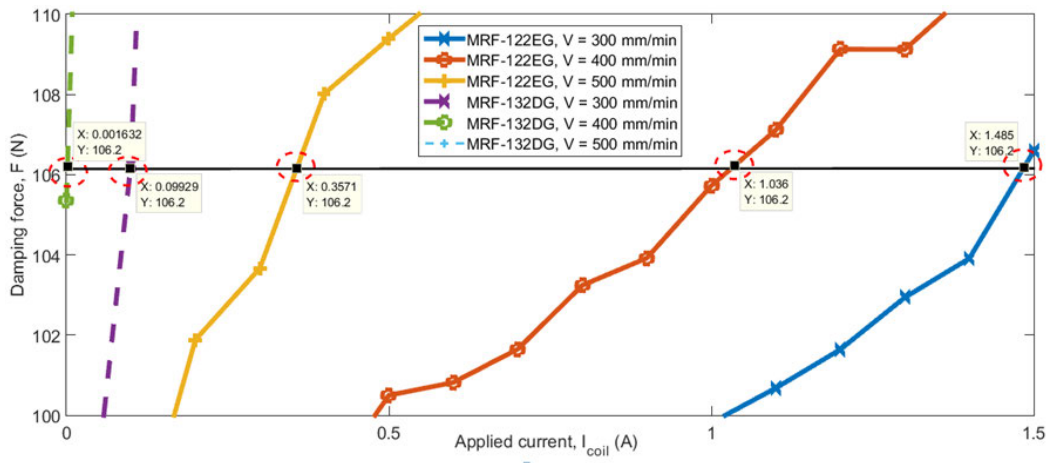


FIGURE 14. Various amounts of current producing 106.2N.

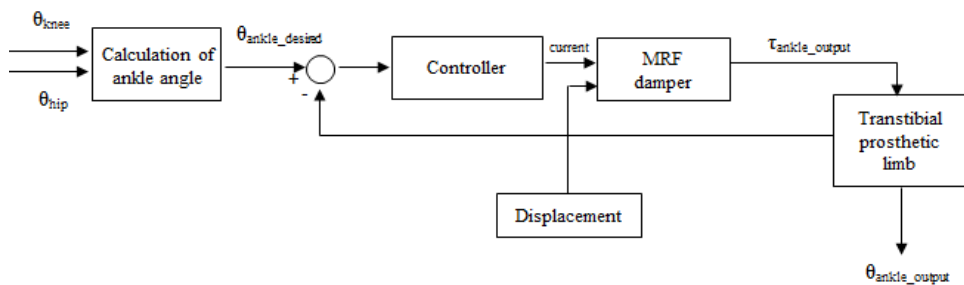


FIGURE 15. Control system block diagram of MRF damper in a prosthetic limb.

a short period, which is about 14% of the total gait cycle. Fuzzy-PID (F-PID) controller adopted in this work has two inputs and three outputs. The inputs to the controller were the error (e) and the rate of change of error (de(t)). On the other hand, the three outputs of the controller were the new gains of K_p , K_i , and K_d . The input and output signals of the system were split into five linguistic variables, namely PB (positive big), PM (positive medium), Z (zero),

NM (negative medium), and NB (negative big). The shape of the membership functions used was in the form of triangular, which is widely practised. The rules governing the controller's decision are listed in Table 4 and are based on the Mamdani type. The range assigned to the input and output of the fuzzy was based on basic knowledge and experience related to the system when designing the PID controller, as in Table 5.

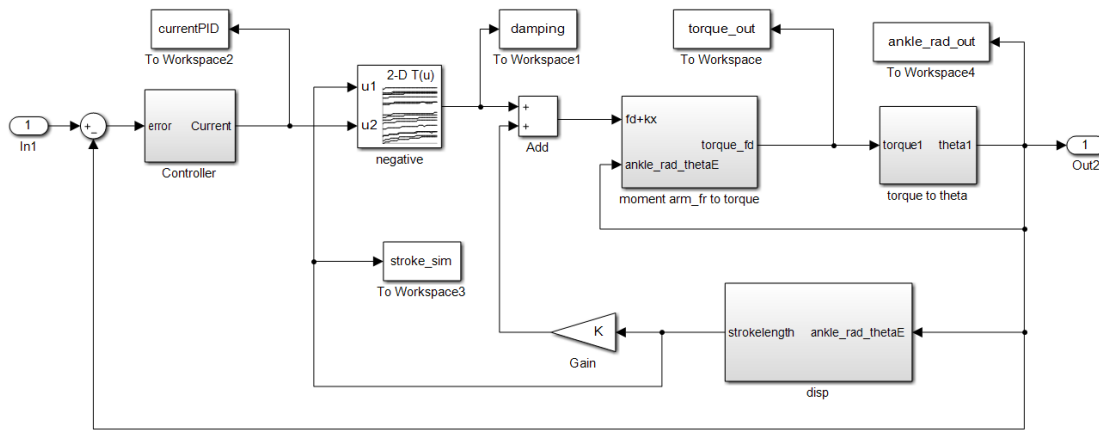


FIGURE 16. Block diagram of the transtibial prosthetic limb in MATLAB Simulink.

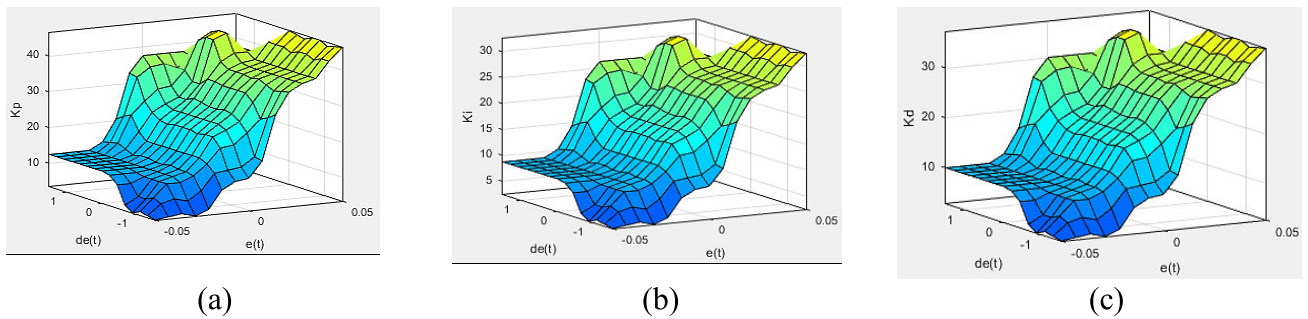


FIGURE 17. Surface plots of the fuzzy governing rules for (a) K_p , (b) K_i and (c) K_d .

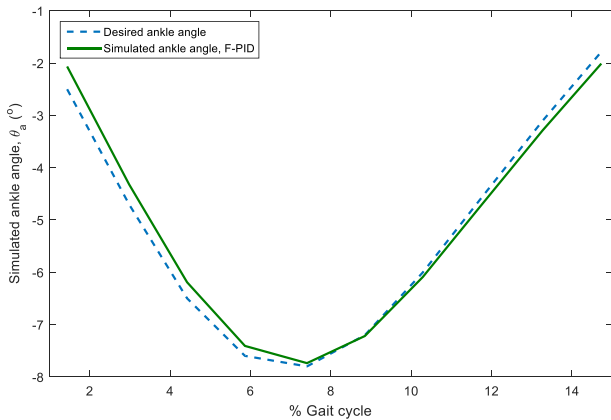


FIGURE 18. Simulated ankle angle with F-PID controller.

The expression relating to the input and output of the controller is in the form of Eq. (8). The rules can be visualized in the surface plots as displayed in Figure 17.

If $e = E_i$ and $de = dE_j$, then:

$$\begin{aligned} K_p &= K_p(i, j), \\ K_i &= K_i(i, j), \\ K_d &= K_d(i, j) \end{aligned} \quad (8)$$

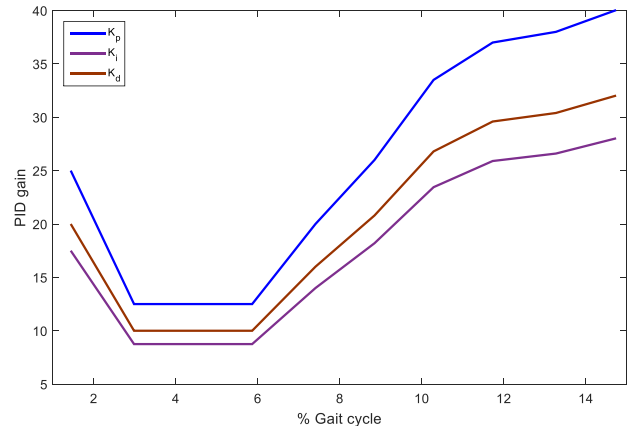


FIGURE 19. The adjusted PID gains.

Figure 18 shows the output of the system. The F-PID controller can minimize the error as the user reaches foot flat. The PID constants changed their values throughout the simulation based on the defined rules, shown in Figure 19. The variations of the constants help ensure the controller's performance, especially during initial contact. The controller's performance is crucial at this stage as the collision between the foot, and the ground happens in a short period, which is about 14% of the total gait cycle.

VI. CONCLUSION AND FUTURE WORK

Overall, this study has investigated the performance of an MRF damper in the development of prosthetic limbs. In this application, the MRF damper acts as a shock absorber to minimize the impact during heel strike and requires current to vary its damping force. The impact force, if not adequately attenuated, might lead to injuries. A Fuzzy PID Control was used to minimize errors. Additionally, a higher percentage of magnetic particles in the fluid has shown an increase in the performance of the MRF damper. At the exact value of stroking velocity, MRF filled with 80.98% of magnetic particles content by weight requires 0.099A, whereby MRF with 72% of solid content by weight needs 1.485A to produce 106.2N, which is the value of damping force required to reduce the impact of transient force in the simulation study.

MRF continues to be investigated and exploited due to versatility in modes of operation controllability in applications such as automotive, aerospace, prosthetics, and medical devices. However, some challenges are still incorporated with the preparation of MRF. Different MRF preparation methods and additive solutions have been explored to enhance their properties and mitigate problems encountered during use. However, research for low-cost solutions for MRF preparation is required; hence MRF can be further employed in different applications. Additionally, a detailed study on the rheological characteristics and damping properties of MRF in the application of prosthetic devices over a long period of use is required to ensure better reliability.

REFERENCES

- N. Konow, E. Azizi, and T. J. Roberts, "Muscle power attenuation by tendon during energy dissipation," *Proc. Roy. Soc. B, Biol. Sci.*, vol. 279, no. 1731, pp. 1108–1113, Mar. 2012.
- M. J. Decker, M. R. Torry, D. J. Wyland, W. I. Sterett, and J. Richard Steadman, "Gender differences in lower extremity kinematics, kinetics and energy absorption during landing," *Clin. Biomech.*, vol. 18, no. 7, pp. 662–669, Aug. 2003.
- Y. Feng and Q. Wang, "Adjusting ankle angle measurement based on a strain gauge bridge for powered transtibial prosthesis," *J. Dyn. Syst., Meas., Control*, vol. 142, no. 7, Jul. 2020, Art. no. 071002.
- H. Huang, D. L. Crouch, M. Liu, G. S. Sawicki, and D. Wang, "A cyber expert system for auto-tuning powered prosthesis impedance control parameters," *Ann. Biomed. Eng.*, vol. 44, no. 5, pp. 1613–1624, May 2016.
- M. R. Tucker, J. Olivier, A. Pagel, H. Bleuler, M. Bourri, O. Lambercy, J. D. R. Millán, R. Riener, H. Vallery, and R. Gassert, "Control strategies for active lower extremity prosthetics and orthotics: A review," *J. Neuro-Eng. Rehabil.*, vol. 12, no. 1, p. 1, 2015.
- B. G. A. Lambrecht and H. Kazerooni, "Design of a semi-active knee prosthesis," in *Proc. IEEE Int. Conf. Robot. Autom.*, May 2009, pp. 639–645.
- M. Tran, L. Gabert, M. Cempini, and T. Lenzi, "A lightweight, efficient fully powered knee prosthesis with actively variable transmission," *IEEE Robot. Autom. Lett.*, vol. 4, no. 2, pp. 1186–1193, Apr. 2019.
- J. Zhao, K. Berns, R. de Souza Baptista, and A. P. L. Bo, "Design of variable-damping control for prosthetic knee based on a simulated biped," in *Proc. IEEE 13th Int. Conf. Rehabil. Robot. (ICORR)*, Jun. 2013, pp. 1–6.
- P. Maroti, P. Varga, H. Abraham, G. Falk, T. Zsebe, Z. Meiszterics, S. Mano, Z. Csernatony, S. Rendeki, and M. Nyitrai, "Printing orientation defines anisotropic mechanical properties in additive manufacturing of upper limb prosthetics," *Mater. Res. Exp.*, vol. 6, no. 3, p. 35403, 2019.
- M. Chavoshian, M. Taghizadeh, and N. Z. Meymian, "Implementation and experimental tests of an impedance control of pneumatic artificial muscles for isokinetic rehabilitation," *Comp. Rendus. Mécanique*, vol. 348, no. 3, pp. 211–233, Sep. 2020.
- P. Cherelle, V. Grosu, A. Matthys, B. Vanderborgh, and D. Lefeber, "Design and validation of the ankle mimicking prosthetic (AMP-) foot 2.0," *IEEE Trans. Neural Syst. Rehabil. Eng.*, vol. 22, no. 1, pp. 138–148, Jan. 2014.
- E. A. Bolivar Nieto, S. Rezazadeh, and R. D. Gregg, "Minimizing energy consumption and peak power of series elastic actuators: A convex optimization framework for elastic element design," *IEEE/ASME Trans. Mechatronics*, vol. 24, no. 3, pp. 1334–1345, Jun. 2019.
- T. Verstraten, J. Geeroms, G. Mathijssen, B. Convens, B. Vanderborgh, and D. Lefeber, "Optimizing the power and energy consumption of powered prosthetic ankles with series and parallel elasticity," *Mechanism Mach. Theory*, vol. 116, pp. 419–432, Oct. 2017.
- J. Geeroms, L. Flynn, R. Jimenez-Fabian, B. Vanderborgh, and D. Lefeber, "Design and energetic evaluation of a prosthetic knee joint actuator with a lockable parallel spring," *Bioinspiration Biomimetics*, vol. 12, no. 2, 2017, Art. no. 026002.
- J. Park, G. H. Yoon, J. W. Kang, and S. B. Choi, "Design and control of a prosthetic leg for above-knee amputees operated in semi-active and active modes," *Smart Mater. Struct.*, vol. 25, no. 8, p. 8500, 2016.
- A. V. Anupama, V. Kumaran, and B. Sahoo, "Magneto-mechanical response of additive-free Fe-based magnetorheological fluids: Role of particle shape and magnetic properties," *Mater. Res. Exp.*, vol. 5, no. 8, 2018, Art. no. 85703.
- S. Sato, T. Uchida, N. Kobayashi, and T. Nakagawa, "Evaluation of an elevator emergency stop device with a magnetorheological fluid damper controlled in conformity with the elevator safety guide," *IEEE Trans. Magn.*, vol. 51, no. 11, pp. 1–4, Nov. 2015.
- A. Milecki and M. Hauke, "Application of magnetorheological fluid in industrial shock absorbers," *Mech. Syst. Signal Process.*, vol. 28, pp. 528–541, Apr. 2012.
- Y. Ding, L. Zhang, H.-T. Zhu, and Z.-X. Li, "A new magnetorheological damper for seismic control," *Smart Mater. Struct.*, vol. 22, no. 11, Nov. 2013, Art. no. 115003.
- Y. Kim and A. A. Mahajan, "Smart control of seismically excited highway bridges," in *Computational Methods in Earthquake Engineering*. Springer, 2017, pp. 387–403, doi: 10.1007/978-3-319-47798-5.
- R. S. Prabakar, C. Sujatha, and S. Narayanan, "Response of a quarter car model with optimal magnetorheological damper parameters," *J. Sound Vibrat.*, vol. 332, no. 9, pp. 2191–2206, Apr. 2013.
- S. Sun, X. Tang, J. Yang, D. Ning, H. Du, S. Zhang, and W. Li, "A new generation of magnetorheological vehicle suspension system with tunable stiffness and damping characteristics," *IEEE Trans. Ind. Informat.*, vol. 15, no. 8, pp. 4696–4708, Aug. 2019.
- T. Fras, L. J. Fras, and N. Faderl, "Rubber and magnetorheological fluid applied as the interlayer in composite armours against high-velocity loadings," *Diagnostyka*, vol. 18, no. 3, pp. 63–68, 2017.
- S. Gürgen and T. Yıldız, "Stab resistance of smart polymer coated textiles reinforced with particle additives," *Compos. Struct.*, vol. 235, Mar. 2020, Art. no. 111812.
- A. K. El Wahed and H. C. Wang, "Performance evaluation of a magnetorheological fluid damper using numerical and theoretical methods with experimental validation," *Frontiers Mater.*, vol. 6, p. 27, Feb. 2019.
- C. Xu, B. Feng, J. Xu, L. Xu, S. Chen, and M. Wang, "Rehabilitation strategies for the lower limb rehabilitation robot with magnetorheological damper," in *Proc. IEEE 8th Joint Int. Inf. Technol. Artif. Intell. Conf. (ITAIC)*, May 2019, pp. 79–84.
- X. Yin, S. Guo, N. Xiao, T. Tamiya, H. Hirata, and H. Ishihara, "Safety operation consciousness realization of a MR fluids-based novel haptic interface for teleoperated catheter minimally invasive neurosurgery," *IEEE/ASME Trans. Mechatronics*, vol. 21, no. 2, pp. 1043–1054, Apr. 2016.
- J. Zheng, Y. Li, J. Wang, E. Shiju, and X. Li, "Accelerated thermal aging of grease-based magnetorheological fluids and their lifetime prediction," *Mater. Res. Exp.*, vol. 5, no. 8, 2018, Art. no. 85702.
- W. Yang, J. Su, D. Wei, Y. Zhang, Y. Chen, Q. Yang, and X. Yang, "Experimental research on energy dissipation based on damping of magnetic fluid," *Mater. Res. Exp.*, vol. 7, no. 10, Oct. 2020, Art. no. 106103.
- F. Gao, Y. N. Liu, and W. H. Liao, "Optimal design of a magnetorheological damper used in smart prosthetic knees," *Smart Mater. Struct.*, vol. 26, no. 3, 2017, Art. no. 35034.
- Q. Fu, D. H. Wang, L. Xu, and G. Yuan, "A magnetorheological damper-based prosthetic knee (MRPK) and sliding mode tracking control method for an MRPK-based lower limb prosthesis," *Smart Mater. Struct.*, vol. 26, no. 4, 2017, Art. no. 45030.

- [32] M. G. E. Moghadam, M. M. Shahmardan, and M. Norouzi, "Dissipative particle dynamics modeling of a mini-MR damper focus on magnetic fluid," *J. Mol. Liquids*, vol. 283, pp. 736–747, Jun. 2019.
- [33] H. Sayyaadi and S. H. Zareh, "A new configuration in a prosthetic knee using of hybrid concept of an MR brake with a T-shaped drum incorporating an arc form surface," *Smart Struct. Syst.*, vol. 17, no. 2, pp. 275–296, Feb. 2016.
- [34] S. Seid, S. Chandramohan, and S. Sujatha, "Optimal design of an MR damper valve for prosthetic knee application," *J. Mech. Sci. Technol.*, vol. 32, no. 6, pp. 2959–2965, Jun. 2018.
- [35] I. Ismail and S. N. Aqida, "Fluid-particle separation of magnetorheological (MR) fluid in MR machining application," *Key Eng. Mater.*, vols. 611–612, pp. 746–755, May 2014.
- [36] S. Chen, J. Huang, K. Jian, and J. Ding, "Analysis of influence of temperature on magnetorheological fluid and transmission performance," *Adv. Mater. Sci. Eng.*, vol. 2015, pp. 1–7, Jan. 2015.
- [37] J. Bajkowski, M. Bajkowski, W. Grzesikiewicz, M. Sofonea, M. Shillor, and R. Zalewski, "Analysis of the dependence between a temperature and working parameters of the MR damper," *Mechanics*, vol. 26, no. 4, 2007. [Online]. Available: <https://journals.bg.agh.edu.pl/MECHANICS/2007-04/mech01.pdf>
- [38] J. S. Kumar, P. S. Paul, G. Raghunathan, and D. G. Alex, "A review of challenges and solutions in the preparation and use of magnetorheological fluids," *Int. J. Mech. Mater. Eng.*, vol. 14, no. 1, pp. 1–18, Dec. 2019.
- [39] G. Hu, F. Liu, Z. Xie, and M. Xu, "Design, analysis, and experimental evaluation of a double coil magnetorheological fluid damper," *Shock Vibrat.*, vol. 2016, pp. 1–12, Jan. 2016.
- [40] S.-L. Nie, D.-K. Xin, H. Ji, and F.-L. Yin, "Optimization and performance analysis of magnetorheological fluid damper considering different piston configurations," *J. Intell. Mater. Syst. Struct.*, vol. 30, no. 5, pp. 764–777, Mar. 2019.
- [41] G. A. Dominguez, M. Kamezaki, M. French, and S. Sugano, "An iterative design methodology for the performance optimisation of magnetorheological piston head configurations," in *Proc. IEEE Int. Conf. Adv. Intell. Mechatronics (AIM)*, Jul. 2016, pp. 228–233.
- [42] H. Krishna, H. Kumar, and K. Gangadharan, "Optimization of magnetorheological damper for maximizing magnetic flux density in the fluid flow gap through FEA and GA approaches," *J. Inst. Eng. (India), Ser. C*, vol. 98, no. 4, pp. 533–539, Aug. 2017.
- [43] T. M. Gurubasavaraju, H. Kumar, and M. Arun, "Optimization of mono-magnetorheological tube damper under shear mode," *J. Brazilian Soc. Mech. Sci. Eng.*, vol. 39, no. 6, pp. 2225–2240, 2017.
- [44] R. Desai and R. V. Upadhyay, "Anomalous increase in the magnetorheological properties of magnetic fluid induced by silica nanoparticles," *Mater. Res. Exp.*, vol. 1, no. 4, 2015, Art. no. 46116.
- [45] Z. Parlak, T. Engin, and I. Çalli, "Optimal design of MR damper via finite element analyses of fluid dynamic and magnetic field," *Mechatronics*, vol. 22, no. 6, pp. 890–903, 2012.
- [46] H. J. Singh, W. Hu, N. M. Wereley, and W. Glass, "Experimental validation of a magnetorheological energy absorber design optimized for shock and impact loads," *Smart Mater. Struct.*, vol. 23, no. 12, Dec. 2014, Art. no. 125033.
- [47] A. J. D. Nanthakumar and J. Jancirani, "Design optimization of magnetorheological damper geometry using response surface method for achieving maximum yield stress," *J. Mech. Sci. Technol.*, vol. 33, no. 9, pp. 4319–4329, Sep. 2019.
- [48] Y. Peng and P. Pei, "Microstructure evolution based particle chain model for shear yield stress of magnetorheological fluids," *J. Intell. Mater. Syst. Struct.*, vol. 32, no. 1, pp. 49–64, Aug. 2020, doi: [10.1177/1045389X20988779](https://doi.org/10.1177/1045389X20988779).
- [49] Y. B. Peng, R. Ghanem, and J. Li, "Investigations of microstructured behaviors of magnetorheological suspensions," *J. Intell. Mater. Syst. Struct.*, vol. 23, no. 12, pp. 1351–1370, May 2012, doi: [10.1177/1045389X12447288](https://doi.org/10.1177/1045389X12447288).
- [50] N. Wang, X. Liu, S. Sun, G. Królczyk, Z. Li, and W. Li, "Microscopic characteristics of magnetorheological fluids subjected to magnetic fields," *J. Magn. Magn. Mater.*, vol. 501, May 2020, Art. no. 166443.
- [51] J. Wu, L. Pei, S. Xuan, Q. Yan, and X. Gong, "Particle size dependent rheological property in magnetic fluid," *J. Magn. Magn. Mater.*, vol. 408, pp. 18–25, Jun. 2016.
- [52] J. S. Kumar, P. S. Paul, G. Raghunathan, and D. G. Alex, "A review of challenges and solutions in the preparation and use of magnetorheological fluids," *Int. J. Mech. Mater. Eng.*, vol. 14, no. 1, p. 13, 2019.



N. H. DIYANA NORDIN received the Ph.D. degree in engineering from International Islamic University Malaysia (IIUM), in 2018. She is an Assistant Professor with the Smart Structures, Systems and Control Research Laboratory, Department of Mechatronics, Kulliyah of Engineering, IIUM. Her research interests include semi-active vibration control, smart materials and applications, and biomechanics.



ASAN G. A. MUTHALIF (Senior Member, IEEE) received the bachelor's and master's degrees in mechatronics engineering from International Islamic University Malaysia (IIUM) and the Ph.D. degree from Cambridge University, in 2008. He is currently an Associate Professor with the Department of Mechanical and Industrial Engineering, Qatar University. His research interests include mechatronics, active & semi-active vibration control, smart materials and structures, vibration-based energy harvesting, mid-high frequency vibration control, statistical energy analysis (SEA), and dynamics of built-up structures.



M. KHUSYAIIE M. RAZALI received the bachelor's and master's degrees in mechatronics engineering from International Islamic University Malaysia (IIUM), in 2015 and 2019, respectively. He worked as a Research Assistant with the Smart Structures, Systems and Control Research Laboratory, Department of Mechatronic Engineering, IIUM. His research interests include mechatronics, vibration control, and smart materials.



ABDELRAHMAN ALI received the bachelor's degree in mechanical engineering from Qatar University, Doha, Qatar, in 2020, where he is currently pursuing the master's degree in mechanical engineering. He is also working as a Graduate Research Assistant with the Mechanical and Industrial Engineering Department, Qatar University. His research interests include active and semi-active vibration control, piezoelectric vibration energy harvesting, smart materials, structures (magnetorheological elastomers and fluids), and finite element analysis.



AYMAN MUSTAFA SALEM received the B.Sc. degree in mechatronics engineering from the Higher Technological Institute (HIT), Egypt, in 2011, and the M.Sc. degree in mechanical engineering from Qatar University, in 2015. He is currently pursuing the Ph.D. degree with the Department of Mechanical Engineering, University of Malaya, Kuala Lumpur. His research interests include controls, mechatronics, manufacturing, and vibration analysis.

...